### Title

Concerted Electron-Nuclear Motion in Proton-Coupled Electron Transfer-Driven Grotthuss-Type Proton Translocation




### Journal

The Journal of Physical Chemistry Letters, 13(20)

### ISSN

1948-7185



### Authors

Arsenault, Eric A
Guerra, Walter D
Shee, James
et al.



### Publication Date

2022-05-26

### DOI

10.1021/acs.jpclett.2c00585

Peer reviewed

THE JOURNAL OF PHYSICAL CHEMISTRY LETTERS
A JOURNAL OF THE AMERICAN CHEMICAL SOCIETY

pubs.acs.org/JPCL

Letter

# Concerted Electron-Nuclear Motion in Proton-Coupled Electron Transfer-Driven Grotthuss-Type Proton Translocation

Eric A. Arsenault,[▽] Walter D. Guerra,[▽] James Shee,[▽] Edgar A. Reyes Cruz,[▽] Yusuke Yoneda, Brian L. Wadsworth, Emmanuel Odella, Maria N. Urrutia, Gerdenis Kodis, Gary F. Moore, Martin Head-Gordon, Ana L. Moore, Thomas A. Moore, and Graham R. Fleming*

Cite This: *J. Phys. Chem. Lett.* 2022, 13, 4479−4485

Read Online

ACCESS | Metrics & More | Article Recommendations | Supporting Information

**ABSTRACT:** Photoinduced proton-coupled electron transfer and long-range two-proton transport via a Grotthuss-type mechanism are investigated in a biomimetic construct. The ultrafast, nonequilibrium dynamics are assessed via two-dimensional electronic vibrational spectroscopy, in concert with electrochemical and computational techniques. A low-frequency mode is identified experimentally and found to promote double proton and electron transfer, supported by recent theoretical simulations of a similar but abbreviated (non-photoactive) system. Excitation frequency peak evolution and center line slope dynamics show direct evidence of strongly coupled nuclear and electronic degrees of freedom, from which we can conclude that the double proton and electron transfer processes are concerted (up to an uncertainty of 24 fs). The nonequilibrium pathway from the photoexcited Franck−Condon region to the E2PT state is characterized by an ∼110 fs time scale. This study and the tools presented herein constitute a new window into hot charge transfer processes involving an electron and multiple protons.

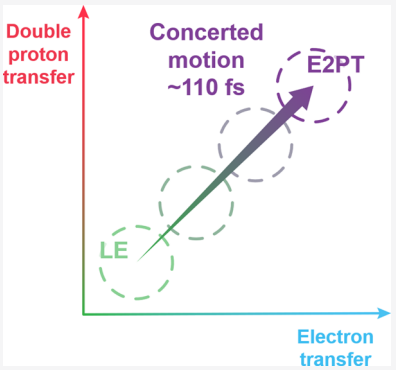


Reversibly coupling the electrochemical potential of redox reactions to the generation of proton-motive force (PMF) is the central principle of bioenergetics in all living organisms.[1] Among a variety of mechanisms for generating PMF, two fundamental processes may be used in series. First, redox reactions involving protons may use proton-coupled electron transfer (PCET) processes, which, in addition to providing kinetically efficient, low-activation energy reaction pathways for protons and electrons, provide a thermodynamically efficient mechanism for coupling electrochemical potential to proton activity.[2−4] Second, by coupling PCET to a Grotthuss-type proton translocation, protons can be efficiently transferred over the nanoscale distances required to span the biological membrane. Examples of PCET can be found in a wide range of biochemical reactions, and Grotthuss-type processes have been suggested as mechanisms for proton transfer in many biological systems.[2−14]

A detailed understanding of how nature accomplishes the efficient conversion of redox potential to PMF via PCET and a Grotthuss-type process is necessary for it to be adapted to reengineered photosynthesis for improved yields.[15−17] In addition, proton control is technologically important for improvements in a wide variety of catalysts.[18,19] Grotthuss-type processes have also been identified as being key to extremely high charge/discharge rates in proton batteries.[20] As the full range of proton-based energy-linked processes in biology becomes better understood and biomimicry becomes more influential in technology, the value of exchanging chemical potential between redox potential and PMF is likely to also find its way into technological applications, enabling cleaner and more efficient processes.

Synchronizing the ensemble by ultrafast optical triggering and simultaneously observing the vibrational markers for electron and proton transfers has the potential to provide new insight into the coupling of PCET and Grotthuss-type processes. Recently, we investigated photodriven PCET in a biomimetic model system with the emerging two-dimensional electronic-vibrational (2DEV) spectroscopic technique[21,22] and electronic structure calculations in which electron transfer and proton transfer were found to occur on a 120 fs time scale accompanied by substantial inner sphere reorganization.[23] In that system, a nonequilibrium PCET pathway was observed and found to correspond to the evolution from the photoexcited, partly charge transferred state to the fully charge separated state accompanied via nuclear rearrangement and solvation. Because the nonequilibrium pathway proceeded without a barrier, it was possible to dynamically track the evolution of the reaction (with the presence of a barrier, only the initial and final states would be significantly populated).

**Received:** February 25, 2022
**Accepted:** May 2, 2022
**Published:** May 14, 2022





https://doi.org/10.1021/acs.jpclett.2c00585
*J. Phys. Chem. Lett.* 2022, 13, 4479−4485

Herein, we investigate a more complicated system in which a similar photodriven PCET process is coupled to a Grotthuss-type proton wire so that a second proton translocation occurs and can be characterized dynamically. The construct is porphyrin-benzimidazole-phenol-pyridine [$PF_{15}$-BIP-Pyr (Scheme 1)]. Upon photoexcitation of the porphyrin moiety, electron transfer (ET) from the phenol to the porphyrin is coupled to both proton transfer from the phenolic proton to benzimidazole and proton transfer from benzimidazole to pyridine (Scheme 1), leading to the formation of a one-electron, two-proton transfer (E2PT) product (*vide infra*). In this work, we leverage the application of 2DEV spectroscopy to elucidate the coupled PCET and Grotthuss-type dynamics leading to the formation of the E2PT product. We focus exclusively on the nonequilibrium pathway and find that the proton translocations are facilitated by a low-frequency vibration of the BIP-Pyr moiety as supported by a recent theoretical investigation.[24] In addition, the presence of the low-frequency modulation allows for a comparison of the phase associated with the spectroscopic signatures tracking electron and proton transfer and provides evidence that E2PT product formation is a concerted process. 2DEV spectroscopy also allows for the correlation between the electronic and nuclear degrees of freedom to be followed directly and is therefore highly sensitive to electronic-vibrational (vibronic) mixing, which is found to play a significant role in the dynamics of this proton wire.

**Scheme 1. Molecular Structure of the Photoinduced Proton Wire ($PF_{15}$-BIP-Pyr)**[a]

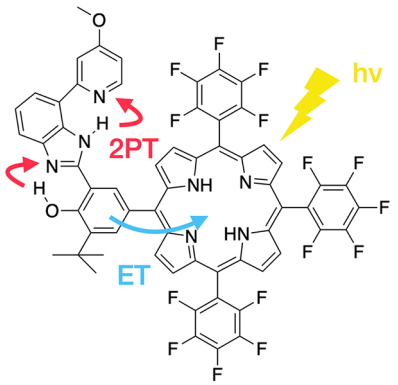


[a]The red arrows indicate the double proton transfer (2PT), and the blue arrow indicates the electron transfer (ET) following photoexcitation ($h\nu$).

Steady state infrared spectroelectrochemical (IRSEC) measurements were performed to examine changes in the IR spectra due to oxidation and reduction of the system (Figure 1) and to facilitate assignments in the 2DEV spectra discussed below. Upon oxidation, new bands at 1636, 1614, and 1535 $cm^{-1}$ appeared (Figure 1a). These frequencies are similar to those observed in pyridinium salts, $C_5H_5NH^+$ (1635, 1610, and 1535 $cm^{-1}$), and are assigned to the $PyrH^+$ ring stretching modes.[25,26] Therefore, these bands serve as markers for double proton transfer (2PT). Upon reduction (Figure 1b), a band at 1593 $cm^{-1}$ emerges, which is assigned to the formation of a porphyrin radical anion as observed in previous studies.[23,27] This band then serves to track ET. The oxidative IRSEC measurements indicate the location of the translocated protons in the E2PT product, and the reductive IRSEC measurements identify the porphyrin radical anion in the E2PT product.

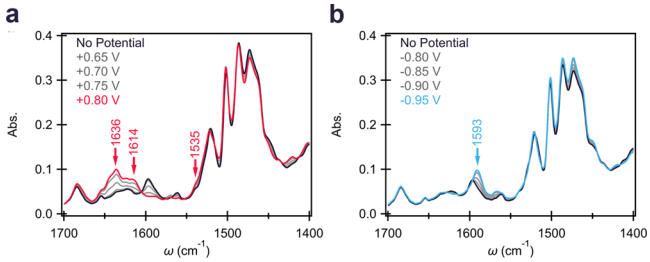


**Figure 1.** IRSEC spectra of $PF_{15}$-BIP-Pyr upon (a) oxidation and (b) reduction. The black curves show the neutral species, and the colored curves show oxidized (red) and reduced species (blue). Spectra were recorded in a dry deuterated acetonitrile solution with 0.1 M $TBAPF_6$. The applied potentials indicated in the figure are vs a silver wire reference electrode (see section 1.2 of the Supporting Information for experimental details).

The midpoint potentials ($E_{1/2}$) for the $PF_{15}$-BIP-$Pyr^+$/$PF_{15}$-BIP-Pyr and $PF_{15}$-BIP-Pyr/$PF_{15}$-BIP-$Pyr^-$ redox couples were estimated to be 0.85 and −0.83 V versus SCE, respectively, by cyclic voltammetry measurements (Figure S2). The $E_{1/2}$ of a reference compound that can undergo only one-electron, one-proton transfer (E1PT) ($BIP^+$-Pyr/BIP-Pyr) was measured to be 1.01 V versus SCE.[28] Assuming the center-to-center distance between the phenol and porphyrin moieties ($l$) to be 6.4 Å and the excited state ($S_1$) energy ($E_{00}$) to be 1.92 eV, the driving force ($\Delta G$) can be estimated to be −300 and −140 meV for the E2PT and E1PT products, respectively (see section 2.1 of the Supporting Information for further details). The differential driving force (between E1PT and E2PT states) obtained electrochemically is consistent with quantum chemical calculations performed on the full $PF_{15}$-BIP-Pyr molecule (see section 3 of the Supporting Information and Table S2). Therefore, only the E2PT product is expected to be populated at thermodynamic equilibrium in these measurements, just as previously determined for BIP-Pyr in a recent study,[28] and as expected on the basis of the IRSEC results presented above.

We now turn to the ultrafast 2DEV measurements (see section 1.4 of the Supporting Information for experimental details). Briefly, in a 2DEV experiment, visible excitation pulses prepare an ensemble of electronic/vibronic states that evolve as a function of waiting time, $T$, which are tracked via an IR detection pulse. The resulting spectra are then presented as (visible) excitation frequency−(IR) detection frequency correlation plots at given waiting times, allowing for the correlation between electronic and vibrational degrees of freedom to be followed directly. This correlation can be quantitatively described by the center line slope (CLS) of the spectral features, which is related to a cross correlation of vibrational and electronic dipoles.[21,29] As a result, this quantity is highly sensitive to both dynamical changes in the electronic structure and the mixing of vibronic states.[23,30−32]

Figure 2 shows representative 2DEV spectra for $PF_{15}$-BIP-Pyr. Immediately after photoexcitation, ground state bleach (GSB) features were observed at 1505, 1524, 1537, and 1564 $cm^{-1}$, while photoinduced absorption (PIA) features were observed at 1514, 1530, 1544, 1586, 1604, 1627, 1648, 1665, 1682, and 1694 $cm^{-1}$. Below ∼1540 $cm^{-1}$, the observed spectral features reflect those of $PF_{15}$.[23] However, distinct bands at 1586, 1604, and 1627 $cm^{-1}$ were observed in the


https://doi.org/10.1021/acs.jpclett.2c00585
J. Phys. Chem. Lett. 2022, 13, 4479−4485

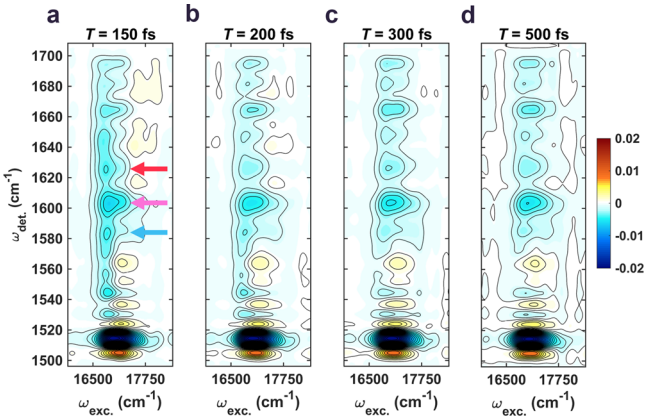


**Figure 2.** (a–d) 2DEV spectra of $PF_{15}$-BIP-Pyr in deuterated acetonitrile at 150, 200, 300, and 500 fs, respectively. Positive signals (red/yellow contours) indicate ground state bleaches, and negative signals (blue contours) represent photoinduced absorptions (PIAs). Contour levels are drawn in 5% intervals. Arrows indicate the main PIA features of interest at 1586 $cm^{-1}$ (ET, blue), 1604 $cm^{-1}$ (2PT, pink), and 1627 $cm^{-1}$ (2PT, red).

2DEV spectra of this species, $PF_{15}$-BIP-Pyr, and are ascribed to ET (1586 $cm^{-1}$) and 2PT (1604 and 1627 $cm^{-1}$) on the basis of the IRSEC measurements, indicating the formation of the E2PT product following photoexcitation. Additional PIAs were observed at >1630 $cm^{-1}$ and are very likely related to the E2PT product on the basis of similarities in the observed dynamics. Although only slight spectral evolution was observed in this region in the IRSEC measurements (Figure 1), the E2PT product in the 2DEV measurements is formed on the excited state potential surface, so we do not expect complete agreement. The dynamics of the features at 1586, 1604, and 1627 $cm^{-1}$, corresponding to the most significant changes in the IRSEC measurements, will be the focus for the remainder of the discussion. We further note that the observed appearance of these bands within ~90 fs (our instrument response function) suggests, on the basis of the free energy difference between E1PT and E2PT products (more driving force for E2PT by ~160 meV), that the E1PT is only transiently formed (<90 fs), if at all. As we will show, analysis of the 2DEV spectral dynamics reveals that it is very unlikely the E1PT product is ever formed.

To understand the dynamics of the ultrafast, nonequilibrium formation of the E2PT product, we first focus on the excitation frequency ($\omega_{exc.}$) peak evolution at specific detection frequencies corresponding to either the 2PT or ET signals (Figure 3a; see Figure S5 for raw data). We find that the $\omega_{exc.}$ peak evolution for these features exhibits significant evolution within the first few hundred femtoseconds (Figure 3a). This is in stark contrast to features that are specific to $PF_{15}$ (1505 and 1514 $cm^{-1}$),[23] not relevant to the E2PT product, which do not show any dynamics along $\omega_{exc.}$ during the waiting time (Figures S5 and S6). The evolution of the 2PT and ET signals, however, is striking in that the $\omega_{exc.}$ peak evolution appears to undergo an ~200 $cm^{-1}$ blue-shift, contradictory to the expected energetic relaxation from the Franck–Condon region due to either electronic or solvent rearrangement. The observed dynamics can be rationalized by viewing the observed $\omega_{exc.}$ peak evolution not as a blue-shift but rather as a result of modulation by a low-frequency vibrational mode. This is reminiscent of a previous 2DEV study that revealed that a low-

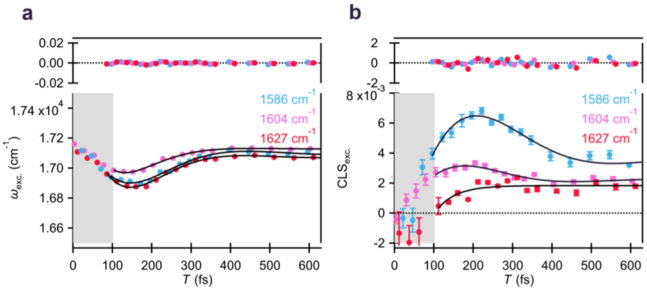


**Figure 3.** (a) $\omega_{exc.}$ peak evolution of $PF_{15}$-BIP-Pyr at 1586 $cm^{-1}$ (ET, blue), 1604 $cm^{-1}$ (2PT, pink), and 1627 $cm^{-1}$ (2PT, red). Solid black lines indicate the fit results (listed in Table 1), and the residuals for each fit are shown above panels a and b. (b) Center line slope (CLS) dynamics of $PF_{15}$-BIP-Pyr at 1586 $cm^{-1}$ (ET, blue), 1604 $cm^{-1}$ (2PT, pink), and 1627 $cm^{-1}$ (2PT, red). Solid black lines indicate the fit results (listed in Table 2). In panels a and b, the time range in which visible and IR pulses overlap, <90 fs, is indicated by the shaded area.

frequency vibrational mode can influence the $\omega_{exc.}$ peak evolution if it is coupled to both the excited electronic state and the probed vibrational mode.[33] Indeed, we find here that the dynamics of the $\omega_{exc.}$ peak evolution fit well and consistently to a damped cosine function (results listed in Table 1) and not to a mono- or biexponential function. From

**Table 1. Parameters from the Fit of $\omega_{exc.}$ Peak Evolution (see Figure 3a) to a Damped Cosine Function $[f = A_0 + A_1 \cos(\omega_1 t + \varphi_1)e^{-t/\tau_1}]$**

| | $A_0$ | $A_1$ | $\omega_1$ ($cm^{-1}$) | $\varphi_1$ (deg) | $\tau_1$ (fs) |
|---|---|---|---|---|---|
| 1586 $cm^{-1}$ (ET) | 17090 | 675 | 56 ± 3 | 57 ± 7 | 140 ± 30 |
| 1604 $cm^{-1}$ (2PT) | 17127 | 1121 | 51 ± 5 | 57 ± 4 | 86 ± 15 |
| 1627 $cm^{-1}$ (2PT) | 17068 | 923 | 58 ± 2 | 49 ± 3 | 110 ± 13 |

Table 1, it is apparent that the three bands yield nearly identical fits, where the average values for the frequency and damping time of this low-frequency mode were found to be 55 ± 2 $cm^{-1}$ and 112 ± 12 fs, respectively.

In a first-principles molecular dynamics study of the nonequilibrium PCET dynamics of a BIP construct by Goings and Hammes-Schiffer, the vibrational modes most crucial to the proton transfer process were predicted.[24] In particular, a slow bending mode in the plane of the BIP subunit, found to dominate the inner sphere reorganization, was identified as the most important vibration for facilitating proton transfer. For the BIP-Pyr species (the one under investigation here but without the $PF_{15}$ group), the frequency of this vibrational mode was determined to be 45 $cm^{-1}$, specifically corresponding to an in-plane bending motion that modulates the PT distances following oxidation. Despite the fact that this investigation features the inclusion of a photoactive, electron-accepting $PF_{15}$ group and is in solution rather than in the gas phase, we nevertheless identify the presence of a low-frequency vibration with a similar frequency, 55 ± 2 $cm^{-1}$, in the dynamics of the nonequilibrium PCET pathway. We therefore assign the observed vibration as an in-plane bend localized on the BIP-Pyr that, when damped, promotes 2PT (where we note that this mode is quite delocalized over the BIP moiety but does not involve the $PF_{15}$ portion of the molecule as is evident from the lack of any $\omega_{exc.}$ peak evolution displayed by modes specific to the $PF_{15}$ moiety as discussed above and


https://doi.org/10.1021/acs.jpclett.2c00585
J. Phys. Chem. Lett. 2022, 13, 4479–4485

shown in Figures S6 and S7). We emphasize that the 55 $cm^{-1}$ mode specifically promotes the formation of the E2PT product (i.e., involves double proton translocation), which suggests that the E1PT product is not formed or at most is only transiently populated during the reaction.

An additional important distinction to note between the previous theoretical study and this experimental work involves the ET process. In the work of Goings and Hammes-Schiffer, the oxidation process was treated by instantaneously removing an electron from the system. However, in the photoactive E2PT species investigated here, the nonequilibrium pathway does not undergo instantaneous ET. Rather, initial photoexcitation corresponds to a $\pi$ to $\pi^*$ electronic transition on the porphyrin, followed by an ultrafast, nonequilibrium evolution of protons and electron density giving rise to the E2PT process (see section 3 of the Supporting Information, Figure S11, and the discussion below). We also find experimentally that both the ET and 2PT features are modulated by the low-frequency mode. In fact, the frequencies and phase shifts extracted from the fit to a damped oscillator are nearly identical (Table 1). The agreement in the phase shift in particular constitutes strong evidence that the transfers of the electron and two protons are concerted, even on ultrafast time scales. In addition, the error in the phase shifts can be used to estimate the degree of concertedness of E2PT product formation. On the basis of the average frequency of the low-frequency mode, 55 ± 2 $cm^{-1}$, and the largest error in the phase, ±7°, we can estimate that the error in the delay between the ET and 2PT features is ∼24 fs, which we interpret to mean that the ultrafast motion of the electron and two protons is concerted within an uncertainty of ∼24 fs.

Turning to the CLS, we can understand how the coupling of this vibration to the E2PT process gives rise to vibronic mixing and influences the correlation between the electronic and vibrational degrees of freedom that are directly interrogated. Figure 3b shows the CLS dynamics of the ET and 2PT features. The CLS dynamics observed are strikingly similar to the $\omega_{exc.}$ peak evolution, notably the modes at 1586 and 1604 $cm^{-1}$. The discrepancy in the CLS dynamics of the feature at 1627 $cm^{-1}$, which we show for the sake of completeness in Table 2, could be due to differences in the degree of coupling between this mode and the low-frequency mode that is known to drastically influence the CLS.[30] Another possibility is that peak overlap from weak positive features just above and below 1627 $cm^{-1}$ could obscure the CLS dynamics of this mode. Both of these possibilities are supported by the fact that there is agreement between the $\omega_{exc.}$ peak evolution for this feature and the modes at 1586 and 1604 $cm^{-1}$ (Table 1) despite the discrepancy in the CLS dynamics. We now focus on the modes at 1586 and 1604 $cm^{-1}$. Utilizing a damped cosine fit function, we obtain an average frequency for the CLS dynamics of 55 ± 9 $cm^{-1}$ and a damping time of 165 ± 60 fs, which are in agreement with the values obtained for $\omega_{exc.}$ peak evolution (see Table 2 for complete fit details). This indicates that the same vibrational mode is driving the CLS as was observed in the $\omega_{exc.}$ peak evolution. Because the CLS is related to a cross correlation of electronic and vibrational dipoles, we can understand the non-zero CLS in this case as arising from vibronic mixing, which significantly alters the transition moments.[23,30] In contrast, the CLSs of the bands specific to $PF_{15}$ (1505 and 1514 $cm^{-1}$),[23] which are not relevant to the E2PT product, were essentially constant over our observation time window (Figure S4). We conclude that the ultrafast Grotthuss-type process in this system is driven by highly correlated electronic and nuclear evolution arising from vibronic mixing.

**Table 2. Parameters from a Fit of CLS Dynamics (see Figure 3b) to a Damped Cosine Function $[f = A_0 + A_1 \cos(\omega_1 t + \varphi_1)e^{-t/\tau_1}]$**

| | $A_0$ | $A_1$ | $\omega_1$ ($cm^{-1}$) | $\varphi_1$ (deg) | $\tau_1$ (fs) |
|---|---|---|---|---|---|
| 1586 $cm^{-1}$ (ET) | 0.27 | 0.73 | 48 ± 8 | 220 ± 10 | 180 ± 50 |
| 1604 $cm^{-1}$ (2PT) | 0.39 | 0.61 | 61 ± 9 | 210 ± 13 | 150 ± 70 |
| 1627 $cm^{-1}$ (2PT)[a] | 0.11 | −0.89 | – | – | 50 ± 23 |

[a]The CLS dynamics for this mode were unable to be fit to a damped cosine function.

Interestingly, the CLS dynamics for this species differ significantly from those observed previously for $PF_{15}$-BIP (an E1PT only system). In that case, the CLS dynamics reflected a monotonic rise on a time scale estimated to be 120 fs that was assigned to the evolution from the Franck−Condon region of the locally excited (LE) state to the minimum of the E1PT state, accompanied by a twisting of the dihedral angle between BIP and porphyrin moieties from 60° to 90°.[23] This dihedral twisting was found to result in an increase in the electronic dipole moment, which in turn drove the observed increase in the CLS. To rationalize and gain further insight into the differences in the PCET reaction in $PF_{15}$-BIP versus $PF_{15}$-BIP-Pyr, dipole moments of the E2PT state of the latter were calculated as a function of the dihedral angle between BIP and porphyrin moieties over the same range (see section 3 of the Supporting Information for further details). One can see that the electronic dipole moment again shows a concomitant increase with the dihedral angle and reaches a maximum at 90°. However, in addition, near the Franck−Condon region (i.e., with the dihedral angle fixed to that of the ground state, ∼60°), 2PT is found to correspond to ∼80% ET. Thus, the E2PT system has a larger degree of charge transfer character near the Franck−Condon region compared to that in $PF_{15}$-BIP (∼50%).[23] Furthermore, the E2PT state is calculated to be exergonic even without substantial dihedral twisting (see section 3 of the Supporting Information for further details). For these reasons, the low-frequency vibration modulating the PT distances is likely more critical for triggering the concerted 2PT and ET reaction than the dihedral twisting, though we find that the latter is still necessary for complete ET (see section 3 of the Supporting Information). Together, we find that significant nuclear rearrangement is necessary for PCET; however, the specific rearrangement appears to be system-specific.

The $PF_{15}$-BIP-Pyr molecule illustrates an optically triggered Grotthus-type mechanism for the transfer of two protons and one electron. As in the case of one-proton, one-electron transfers (PCETs),[23] we find an ultrafast, nonequilibrium channel for E2PT in this work, enabling the reaction to be followed in real time (cartoon representation shown in Figure 4). No evidence is found for a single proton transfer intermediate, and the process is facilitated by a low-frequency mode as suggested by Goings and Hammes-Schiffer in a recent theoretical study of a related molecule.[24] This modulation of the interproton distances produces a damped cosinusoidal oscillation of the mid-IR modes assigned to the 2PT and ET


https://doi.org/10.1021/acs.jpclett.2c00585
J. Phys. Chem. Lett. 2022, 13, 4479−4485

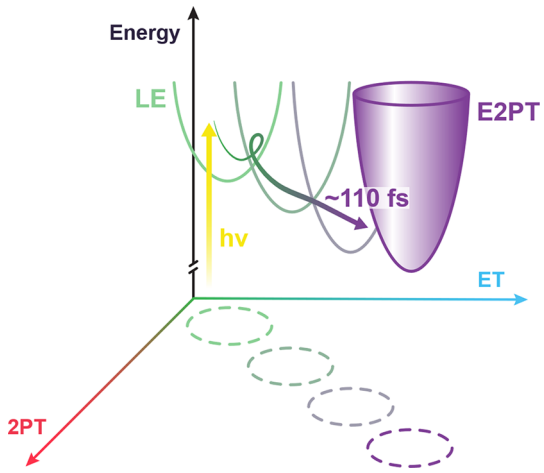


**Figure 4.** Cartoon schematic of the ultrafast, nonequilibrium dynamics of the Grotthus-type proton wire as a function of the double proton transfer (2PT) and electron transfer (ET) coordinates. Following photoexcitation (yellow arrow), the system is led to the unrelaxed Franck−Condon region where concerted 2PT and ET lead to formation of the E2PT product on the ∼110 fs time scale. The concerted electron-nuclear motion is promoted by the damping (purple end of the arrow) of a low-frequency vibration (green end of the arrow) localized in the BIP-Pyr moiety.

components of the E2PT process, clearly demonstrating the involvement of vibronic coupling in the dynamics. Fits of the $\omega_{exc.}$ peak evolution for the modes tracking 2PT and ET reveal identical (within error) phases for the low-frequency oscillation. This, in turn, enables an estimate of the maximum possible delay between the ET and 2PT processes, i.e., the degree to which the ET and 2PT processes are concerted. The error bounds on the phase in Table 1 have a maximum value of ±7°, which given the frequency of ∼55 $cm^{-1}$, translates to a maximum delay of ∼24 fs between the ET and 2PT processes. A more precise delineation of "concertedness" is likely not warranted because the electron distribution progressively evolves until it roughly corresponds to one whole electron transferred to the porphyrin moiety, as also discussed in our recent work.[23] Although not reported at this time, photochemically driven translocations over nanoscale distances should be possible in extended versions of this genre of constructs, and further spectroscopic studies are likely to significantly advance our understanding of the dynamics governing such systems if an optical trigger can be incorporated.[24,34−39]

## ■ ASSOCIATED CONTENT

### Supporting Information

The Supporting Information is available free of charge at https://pubs.acs.org/doi/10.1021/acs.jpclett.2c00585.

Experimental and theoretical methods (including synthesis, IRSEC, cyclic voltammetry, 2DEV spectroscopy, and electronic structure calculations), experimental results (including electrochemical characterization, electronic absorption and laser spectrum, and further center line slope and excitation frequency peak evolution analysis), and computational results (PDF)

## ■ AUTHOR INFORMATION


### Corresponding Author

**Graham R. Fleming** − *Department of Chemistry, University of California, Berkeley, California 94720, United States; Molecular Biophysics and Integrated Bioimaging Division, Lawrence Berkeley National Laboratory, Berkeley, California 94720, United States; Kavli Energy Nanoscience Institute at Berkeley, Berkeley, California 94720, United States;* orcid.org/0000-0003-0847-1838; Email: grfleming@lbl.gov

### Authors

**Eric A. Arsenault** − *Department of Chemistry, University of California, Berkeley, California 94720, United States; Molecular Biophysics and Integrated Bioimaging Division, Lawrence Berkeley National Laboratory, Berkeley, California 94720, United States; Kavli Energy Nanoscience Institute at Berkeley, Berkeley, California 94720, United States;* orcid.org/0000-0002-5363-3229

**Walter D. Guerra** − *School of Molecular Sciences, Arizona State University, Tempe, Arizona 85287, United States;* orcid.org/0000-0003-0712-2740

**James Shee** − *Department of Chemistry, University of California, Berkeley, California 94720, United States; Chemical Sciences Division, Lawrence Berkeley National Laboratory, Berkeley, California 94720, United States;* orcid.org/0000-0001-8333-8151

**Edgar A. Reyes Cruz** − *School of Molecular Sciences, Arizona State University, Tempe, Arizona 85287, United States; The Biodesign Institute Center for Applied Structural Discovery (CASD), Tempe, Arizona 85287, United States;* orcid.org/0000-0001-7307-7613

**Yusuke Yoneda** − *Department of Chemistry, University of California, Berkeley, California 94720, United States; Molecular Biophysics and Integrated Bioimaging Division, Lawrence Berkeley National Laboratory, Berkeley, California 94720, United States; Kavli Energy Nanoscience Institute at Berkeley, Berkeley, California 94720, United States;* Present Address: Y.Y.: Research Center of Integrative Molecular Systems, Institute for Molecular Science, National Institute of Natural Sciences, Okazaki, Aichi 444−8585, Japan; orcid.org/0000-0003-4974-6842

**Brian L. Wadsworth** − *School of Molecular Sciences, Arizona State University, Tempe, Arizona 85287, United States; The Biodesign Institute Center for Applied Structural Discovery (CASD), Tempe, Arizona 85287, United States;* orcid.org/0000-0002-0274-9993

**Emmanuel Odella** − *School of Molecular Sciences, Arizona State University, Tempe, Arizona 85287, United States;* orcid.org/0000-0002-7021-400X

**Maria N. Urrutia** − *School of Molecular Sciences, Arizona State University, Tempe, Arizona 85287, United States;* orcid.org/0000-0003-4274-9688

**Gerdenis Kodis** − *School of Molecular Sciences, Arizona State University, Tempe, Arizona 85287, United States; The Biodesign Institute Center for Applied Structural Discovery (CASD), Tempe, Arizona 85287, United States*

**Gary F. Moore** − *School of Molecular Sciences, Arizona State University, Tempe, Arizona 85287, United States; The Biodesign Institute Center for Applied Structural Discovery (CASD), Tempe, Arizona 85287, United States;* orcid.org/0000-0003-3369-9308




https://doi.org/10.1021/acs.jpclett.2c00585
J. Phys. Chem. Lett. 2022, 13, 4479−4485

**Martin Head-Gordon** − *Department of Chemistry, University of California, Berkeley, California 94720, United States; Chemical Sciences Division, Lawrence Berkeley National Laboratory, Berkeley, California 94720, United States;* orcid.org/0000-0002-4309-6669

**Ana L. Moore** − *School of Molecular Sciences, Arizona State University, Tempe, Arizona 85287, United States;* orcid.org/0000-0002-6653-9506

**Thomas A. Moore** − *School of Molecular Sciences, Arizona State University, Tempe, Arizona 85287, United States;* orcid.org/0000-0002-1577-7117

Complete contact information is available at: https://pubs.acs.org/10.1021/acs.jpclett.2c00585

### Author Contributions

[▽]E.A.A., W.D.G., J.S., and E.A.R.C. contributed equally to this work.

### Notes

The authors declare no competing financial interest.

## ■ ACKNOWLEDGMENTS

This research was supported by the U.S. Department of Energy, Office of Science, Basic Energy Sciences, Chemical Sciences, Geosciences, and Biosciences Division: G.R.F. (FWP 449A), M.H.-G. (DEAC02 05CH11231), T.A.M. and A.L.M. (DE-FG02-03ER15393), and G.F.M. (DE-SC0021186). Y.Y. appreciates the support of the Japan Society for the Promotion of Science (JSPS) Postdoctoral Fellowship for Research Abroad. E.A.A. acknowledges the support of the National Science Foundation Graduate Research Fellowship (Grant DGE 1752814). J.S. acknowledges funding from the National Institute of General Medical Sciences of the National Institutes of Health under Grant F32GM142231. G.F.M. acknowledges support from the Camille Dreyfus Teacher-Scholar Awards Program.

## ■ REFERENCES

(1) Mitchell, P. Coupling of Phosphorylation to Electron and Hydrogen Transfer by a Chemi-Osmotic Type of Mechanism. *Nature.* **1961**, *191*, 144−148.

(2) Migliore, A.; Polizzi, N. F.; Therien, M. J.; Beratan, D. N. Biochemistry and Theory of Proton-Coupled Electron Transfer. *Chem. Rev.* **2014**, *114*, 3381−3465.

(3) Hammes-Schiffer, S.; Soudackov, A. V. Proton-Coupled Electron Transfer in Solution, Proteins, and Electrochemistry. *J. Phys. Chem. B* **2008**, *112*, 14108−14123.

(4) Huynh, M. H. V; Meyer, T. J. Proton-Coupled Electron Transfer. *Chem. Rev.* **2007**, *107*, 5004−5064.

(5) Stubbe, J. A.; Nocera, D. G.; Yee, C. S.; Chang, M. C. Y. Radical Initiation in the Class I Ribonucleotide Reductase: Long-Range Proton-Coupled Electron Transfer? *Chem. Rev.* **2003**, *103*, 2167−2201.

(6) Cukierman, S. Et Tu, Grotthuss! And Other Unfinished Stories. *Biochim. Biophys. Acta - Bioenerg.* **2006**, *1757*, 876−885.

(7) Pavošević, F.; Culpitt, T.; Hammes-Schiffer, S. Multicomponent Quantum Chemistry: Integrating Electronic and Nuclear Quantum Effects via the Nuclear−Electronic Orbital Method. *Chem. Rev.* **2020**, *120*, 4222−4253.

(8) Barry, B. A. Reaction Dynamics and Proton Coupled Electron Transfer: Studies of Tyrosine-Based Charge Transfer in Natural and Biomimetic Systems. *Biochim. Biophys. Acta - Bioenerg.* **2015**, *1847*, 46−54.

(9) Meyer, T. J.; Huynh, M. H. V.; Thorp, H. H. The Possible Role of Proton-Coupled Electron Transfer (PCET) in Water Oxidation by Photosystem II. *Angew. Chemie - Int. Ed.* **2007**, *46*, 5284−5304.

(10) Reece, S. Y.; Nocera, D. G. Proton-Coupled Electron Transfer in Biology: Results from Synergistic Studies in Natural and Model Systems. *Annu. Rev. Biochem.* **2009**, *78*, 673−699.

(11) Nagao, R.; Ueoka-Nakanishi, H.; Noguchi, T. D1-Asn-298 in Photosystem II Is Involved in a Hydrogen-Bond Network near the Redox-Active Tyrosine YZ for Proton Exit during Water Oxidation. *J. Biol. Chem.* **2017**, *292*, 20046−20057.

(12) Kawashima, K.; Saito, K.; Ishikita, H. Mechanism of Radical Formation in the H-Bond Network of D1-Asn298 in Photosystem II. *Biochemistry* **2018**, *57*, 4997−5004.

(13) Vinyard, D. J.; Brudvig, G. W. Progress Toward a Molecular Mechanism of Water Oxidation in Photosystem II. *Annu. Rev. Phys. Chem.* **2017**, *68*, 101−116.

(14) Saito, K.; Rutherford, A. W.; Ishikita, H. Energetics of Proton Release on the First Oxidation Step in the Water-Oxidizing Enzyme. *Nat. Commun.* **2015**, *6*, 8488.

(15) Long, S. P.; Marshall-Colon, A.; Zhu, X. G. Meeting the Global Food Demand of the Future by Engineering Crop Photosynthesis and Yield Potential. *Cell* **2015**, *161*, 56−66.

(16) Blankenship, R. E.; Tiede, D. M.; Barber, J.; Brudvig, G. W.; Fleming, G.; Ghirardi, M.; Gunner, M. R.; Junge, W.; Kramer, D. M.; Melis, A.; Moore, T. A.; Moser, C. C.; Nocera, D. G.; Nozik, A. J.; Ort, D. R.; Parson, W. W.; Prince, R. C.; Sayre, R. T. Comparing Photosynthetic and Photovoltaic Efficiencies and Recognizing the Potential for Improvement. *Science.* **2011**, *332*, 805−809.

(17) Ort, D. R.; Merchant, S. S.; Alric, J.; Barkan, A.; Blankenship, R. E.; Bock, R.; Croce, R.; Hanson, M. R.; Hibberd, J. M.; Long, S. P.; Moore, T. A.; Moroney, J.; Niyogi, K. K.; Parry, M. A. J.; Peralta-Yahya, P. P.; Prince, R. C.; Redding, K. E.; Spalding, M. H.; Van Wijk, K. J.; Vermaas, W. F. J.; Von Caemmerer, S.; Weber, A. P. M.; Yeates, T. O.; Yuan, J. S.; Zhu, X. G. Redesigning Photosynthesis to Sustainably Meet Global Food and Bioenergy Demand. *Proc. Natl. Acad. Sci. U. S. A.* **2015**, *112*, 8529−8536.

(18) Sayre, H. J.; Tian, L.; Son, M.; Hart, S. M.; Liu, X.; Arias-Rotondo, D. M.; Rand, B. P.; Schlau-Cohen, G. S.; Scholes, G. D. Solar Fuels and Feedstocks: The Quest for Renewable Black Gold. *Energy Environ. Sci.* **2021**, *14*, 1402−1419.

(19) Sayre, H.; Ripberger, H. H.; Odella, E.; Zieleniewska, A.; Heredia, D. A.; Rumbles, G.; Scholes, G. D.; Moore, T. A.; Moore, A. L.; Knowles, R. R. PCET-Based Ligand Limits Charge Recombination with an Ir(III) Photoredox Catalyst. *J. Am. Chem. Soc.* **2021**, *143*, 13034−13043.

(20) Wu, X.; Hong, J. J.; Shin, W.; Ma, L.; Liu, T.; Bi, X.; Yuan, Y.; Qi, Y.; Surta, T. W.; Huang, W.; Neuefeind, J.; Wu, T.; Greaney, P. A.; Lu, J.; Ji, X. Diffusion-Free Grotthuss Topochemistry for High-Rate and Long-Life Proton Batteries. *Nat. Energy 2019 42* **2019**, *4*, 123−130.

(21) Arsenault, E. A.; Bhattacharyya, P.; Yoneda, Y.; Fleming, G. R. Two-Dimensional Electronic-Vibrational Spectroscopy: Exploring the Interplay of Electrons and Nuclei in Excited State Molecular Dynamics. *J. Chem. Phys.* **2021**, *155*, 020901.

(22) Oliver, T. A. A.; Lewis, N. H. C.; Fleming, G. R. Correlating the Motion of Electrons and Nuclei with Two-Dimensional Electronic−Vibrational Spectroscopy. *Proc. Natl. Acad. Sci. U. S. A.* **2014**, *111*, 10061−10066; Correction for Oliver et al., Correlating the motion of electrons and nuclei with two-dimensional electronic−vibrational spectroscopy. *Proc. Natl. Acad. Sci. U. S. A.* **2014**, *111*, 16628−16629.

(23) Yoneda, Y.; Mora, S. J.; Shee, J.; Wadsworth, B. L.; Arsenault, E. A.; Hait, D.; Kodis, G.; Gust, D.; Moore, G. F.; Moore, A. L.; Head-Gordon, M.; Moore, T. A.; Fleming, G. R. Electron−Nuclear Dynamics Accompanying Proton-Coupled Electron Transfer. *J. Am. Chem. Soc.* **2021**, *143*, 3104−3112.

(24) Goings, J. J.; Hammes-Schiffer, S. Nonequilibrium Dynamics of Proton-Coupled Electron Transfer in Proton Wires: Concerted but Asynchronous Mechanisms. *ACS Cent. Sci.* **2020**, *6*, 1594−1601.

(25) Cook, D. Vibrational Spectra of Pyridinium Salts*Can. J. Chem.* **1961**, *39*, 2009−2024.

(26) Glazunov, V. P.; Odinokov, S. E. Infrared Spectra of Pyridinium Salts in Solution-I. The Region of Middle Frequencies. *Spectrochim. Acta Part A Mol. Spectrosc.* **1982**, *38*, 399−408.
(27) Moore, G. F.; Hambourger, M.; Gervaldo, M.; Poluektov, O. G.; Rajh, T.; Gust, D.; Moore, T. A.; Moore, A. L. A Bioinspired Construct That Mimics the Proton Coupled Electron Transfer between P680•+ and the Tyrz-His190 Pair of Photosystem II. *J. Am. Chem. Soc.* **2008**, *130*, 10466−10467.
(28) Guerra, W. D.; Odella, E.; Secor, M.; Goings, J. J.; Urrutia, M. N.; Wadsworth, B. L.; Gervaldo, M.; Sereno, L. E.; Moore, T. A.; Moore, G. F.; Hammes-Schiffer, S.; Moore, A. L. Role of Intact Hydrogen-Bond Networks in Multiproton-Coupled Electron Transfer. *J. Am. Chem. Soc.* **2020**, *142*, 21842−21851.
(29) Cho, M.; Fleming, G. R. Two-Dimensional Electronic-Vibrational Spectroscopy Reveals Cross-Correlation between Solvation Dynamics and Vibrational Spectral Diffusion. *J. Phys. Chem. B* **2020**, *124*, 11222−11235.
(30) Arsenault, E. A.; Yoneda, Y.; Iwai, M.; Niyogi, K. K.; Fleming, G. R. Vibronic Mixing Enables Ultrafast Energy Flow in Light-Harvesting Complex II. *Nat. Commun.* **2020**, *11*, 1460.
(31) Wu, E. C.; Ge, Q.; Arsenault, E. A.; Lewis, N. H. C.; Gruenke, N. L.; Head-Gordon, M.; Fleming, G. R. Two-Dimensional Electronic-Vibrational Spectroscopic Study of Conical Intersection Dynamics: An Experimental and Electronic Structure Study. *Phys. Chem. Chem. Phys.* **2019**, *21*, 14153−14163.
(32) Roy, P. P.; Shee, J.; Arsenault, E. A.; Yoneda, Y.; Feuling, K.; Head-Gordon, M.; Fleming, G. R. Solvent Mediated Excited State Proton Transfer in Indigo Carmine. *J. Phys. Chem. Lett.* **2020**, *11*, 4156−4162.
(33) Arsenault, E. A.; Yoneda, Y.; Iwai, M.; Niyogi, K. K.; Fleming, G. R. The Role of Mixed Vibronic Qy-Qx States in Green Light Absorption of Light-Harvesting Complex II. *Nat. Commun.* **2020**, *11*, 6011.
(34) Odella, E.; Mora, S. J.; Wadsworth, B. L.; Huynh, M. T.; Goings, J. J.; Liddell, P. A.; Groy, T. L.; Gervaldo, M.; Sereno, L. E.; Gust, D.; Moore, T. A.; Moore, G. F.; Hammes-Schiffer, S.; Moore, A. L. Controlling Proton-Coupled Electron Transfer in Bioinspired Artificial Photosynthetic Relays. *J. Am. Chem. Soc.* **2018**, *140*, 15450−15460.
(35) Odella, E.; Wadsworth, B. L.; Mora, S. J.; Goings, J. J.; Huynh, M. T.; Gust, D.; Moore, T. A.; Moore, G. F.; Hammes-Schiffer, S.; Moore, A. L. Proton-Coupled Electron Transfer Drives Long-Range Proton Translocation in Bioinspired Systems. *J. Am. Chem. Soc.* **2019**, *141*, 14057−14061.
(36) Mora, S. J.; Heredia, D. A.; Odella, E.; Vrudhula, U.; Gust, D.; Moore, T. A.; Moore, A. L. Design and Synthesis of Benzimidazole Phenol-Porphyrin Dyads for the Study of Bioinspired Photoinduced Protoncoupled Electron Transfer. *J. Porphyr. Phthalocyanines* **2019**, *23*, 1336−1345.
(37) Odella, E.; Mora, S. J.; Wadsworth, B. L.; Goings, J. J.; Gervaldo, M. A.; Sereno, L. E.; Groy, T. L.; Gust, D.; Moore, T. A.; Moore, G. F.; Hammes-Schiffer, S.; Moore, A. L. Proton-Coupled Electron Transfer across Benzimidazole Bridges in Bioinspired Proton Wires. *Chem. Sci.* **2020**, *11*, 3820−3828.
(38) Mora, S. J.; Odella, E.; Moore, G. F.; Gust, D.; Moore, T. A.; Moore, A. L. Proton-Coupled Electron Transfer in Artificial Photosynthetic Systems. *Acc. Chem. Res.* **2018**, *51*, 445−453.
(39) Huynh, M. T.; Mora, S. J.; Villalba, M.; Tejeda-Ferrari, M. E.; Liddell, P. A.; Cherry, B. R.; Teillout, A. L.; MacHan, C. W.; Kubiak, C. P.; Gust, D.; Moore, T. A.; Hammes-Schiffer, S.; Moore, A. L. Concerted One-Electron Two-Proton Transfer Processes in Models Inspired by the Tyr-His Couple of Photosystem II. *ACS Cent. Sci.* **2017**, *3*, 372−380.



https://doi.org/10.1021/acs.jpclett.2c00585
*J. Phys. Chem. Lett.* 2022, 13, 4479−4485